ACS APPLIED MATERIALS & INTERFACES

Research Article

www.acsami.org

Evaluation of the Antibacterial Activity and Biocompatibility for Silver Nanoparticles Immobilized on Nano Silicate Platelets

Jiang-Jen Lin, Wen-Chun Lin, Shing-Da Li, Cheng-Yen Lin, and Shan-hui Hsu*

Institute of Polymer Science and Engineering, National Taiwan University, No. 1, Sec. 4, Roosevelt Road, Taipei, Taiwan, P. R. China

Supporting Information

ABSTRACT: Silver nanoparticles (AgNPs) are known for their bactericidal abilities. The antibacterial potency is dependent on the particle size and dispersion status. In this study, we synthesized AgNP/NSP nanohybrids in two different weight ratios (1/99 and 8/92) using the fully exfoliated clay, i.e., nanosilicate platelets (NSP), as a dispersing agent and carrier for AgNPs. Due to the size of NSP, the immobilized AgNPs do not enter cells readily, which may lower the risk associated with the cellular uptake of AgNPs. The biocompatibility, immunological response, and antimicrobial activities of AgNP/NSP hybrids were evaluated. The results revealed that AgNP/NSP hybrids elicited merely mild inflammatory response and retained the outstanding antibacterial activity. The hybrids were further embedded in poly(ether)urethane (PEU) to increase the biocompatibility. At the same silver content (20 ppm), the PEU-AgNP/NSP nanocomposites were nontoxic to mouse skin fibroblasts, while simultaneously exhibiting nearly complete bacterial growth reduction (99.9%). PEU containing the same amount of free AgNPs did not display such an effect. Our results verify the better biosafety of the AgNPs/NSP hybrids and their polymer nanocomposites for further clinical use.

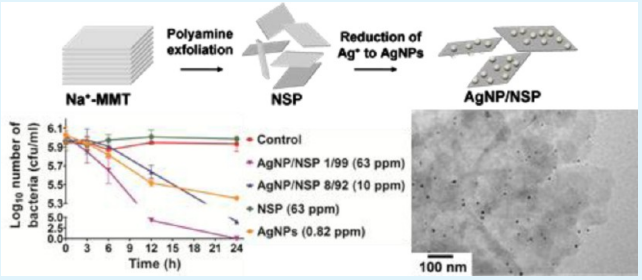

KEYWORDS: *nanosilicate platelets (NSP), silver nanoparticles (AgNPs), antibacterial activity, biocompatibility, nanocomposites, polyurethane*

1. INTRODUCTION

Silver nanoparticles (AgNPs) have attracted considerable interests because of their antimicrobial activities. They have been used in several biomedical products, including wound or burn dressings, catheters, and bone cement.[1−3] The antibacterial effect of AgNPs is proposed to arise from the release of silver ions or alternatively from oxidation.[4,5] Silver ions are known to cause damages to bacterial DNA, proteins, enzymes, as well as the bacterial cell wall.[6−8] AgNPs can directly inhibit bacteria growth by interacting with the cell wall and gradually destroying the metabolic responses.[9,10] Especially, induction of the reactive oxygen species (ROS) is a mechanism responsible for both the antibacterial effect of AgNPs and AgNP-mediated cytotoxicity in different cells.[11−13]

The physicochemical characteristics of AgNPs such as particle size, size distribution, shape, dispersion, and stability are important factors to concern in order to achieve a high antimicrobial performance. Polymeric stabilizers such as polyvinylpyrrolidone,[14] polyvinyl alcohol,[15] polyethylene glycol,[16] gelatin,[17] and starch[18] are commonly used to stabilize AgNPs. These polymers possess certain functional groups that can bind and cover the AgNPs, preventing them from aggregation and controlling their particle size and shape. However, capping AgNPs with organic stabilizers may have a negative influence on the surface activities of AgNPs. The properties and functions of the AgNPs, especially those associated with antibacterial and antimicrobial activities, may also be decreased as a result.[19] Although AgNPs can be used to control infection, they can also enter mammalian cells and cause genotoxicty.[12,20] This raises serious concerns regarding the biosafety of AgNPs.

Recent reports demonstrated that the silica-based nanomaterials, including colloidal, sol−gel, and mesoporous silica nanoparticles, have attracted special attention.[21−23] With the easily modified and controlled surface properties, the nanostructure silica materials are potential candidate materials in sensors, markers and environmental applications.[24,25] Furthermore, the characteristics of silica-based nanomaterials, including nontoxic nature and good biocompatibility, equip them with possible biotechnological applications, particularly in drug delivery systems.[26] Inorganic smectite clays such as montmorillonite (MMT) are naturally abundant and widely applied for pharmaceutical usage because of the swelling and ionic exchange properties.[27−29] MMT is composed of multilayered silicate platelets which are bound by ionic attraction. Recently, the layered structure of Na^+-MMT was successfully delaminated and rendered into individual nanosilicate platelets (abbreviated as NSP) by an exfoliation process. This process involved the use of synthesized polyamines as the exfoliating agent for Na^+-MMT ionic exchange.[30] Because of their

Received: October 31, 2012
Accepted: December 27, 2012
Published: December 27, 2012

relatively larger size (~100 × 100 × 1 nm^3) and abundant negative charge on the surface,[31] NSP are not endocytosed by cells, nor do they exhibit genotoxicity.[32] Besides, the exfoliated state of NSP provides easier accessibility for surface modification in developing silicate nanocomposites. For example, NSP may be utilized for the immobilization of silver nanoparticles (AgNP/NSP).[33] Using NSP to carry and disperse AgNPs may have certain advantages over the polymer-stabilized AgNPs because NSP may interact with but not enter the host cells. Furthermore, no capping agent is required and therefore the surface activities of AgNPs are not adversely affected.

In this study, AgNP/NSP hybrids in two different weight ratios (1/99 and 8/92) were first prepared. The size and zeta potential of the nanohybrids were characterized. The biocompatibility, immunological response, and antimicrobial activities of AgNP/NSP were also evaluated. We sought to determine if the AgNP/NSP hybrids may possess better safety than AgNPs while keeping strong antimicrobial activities. To further increase the biosafety, AgNP/NSP was blended into waterborne poly(ether)urethane (PEU). Previous studies showed that blending AgNPs to waterborne PEU may promote the antimicrobial activity as well as reduce the inflammatory respons.[34] We expected that AgNPs carried by NSP would be better dispersed in PEU than AgNPs, giving rise to outstanding antimicrobial activity as well as improved biocompatibility.

2. EXPERIMENTAL SECTION

2.1. Preparation and Characterization of AgNP/NSP. NSP were prepared from a Na^+ type of layered smectite clay, sodium montmorillonite (Na^+-MMT, supplied by Nanocor Co.), according to the previous literature.[30−32] The cationic exchange capacity (CEC) of Na^+-MMT was 1.20 mequiv/g. After the exfoliation process, the average platelet dimension of each NSP was about 100 × 100 × 1 nm^3. In this study, AgNP/NSP hybrids in two different weight ratios (1/99 and 8/92) were prepared by the following procedures. The AgNP/NSP at 1/99 weight ratio was abbreviated as AgNP/NSP 1/99, and the AgNP/NSP at 8/92 weight ratio abbreviated as AgNP/NSP 8/92. The component of AgNP/NSP was based on the dry weight of NSP and AgNPs. To prepare AgNP/NSP 1/99, NSP (9.96 g, 9.94 wt % in water) were first swollen in deionized water to reach a final concentration of 2 wt %, and followed by the addition of ethanol (49.5 mL) as reducing agent. The reaction mixture was stirred at 300−600 rpm for half an hour. $AgNO_3$ solution (0.016 g of 1.0 wt % in water) was then added to the mixture, in which silver ions were replaced sodium ions in the clay. For preparation of AgNP/NSP 8/92, we dispersed NSP (9.36 g, 9.94 wt % in water) in deionized water to reach 2% final concentration, and added 49.5 mL of ethanol to the solution. After that, $AgNO_3$ solution (0.11 g) was dispersed to 1 wt % in water and added into the reaction mixture. The mixture was heated to 80 °C for 3 h and monitored by UV−vis spectroscopy and observed the color change from yellow to deepred, indicating the reduction of Ag^+ to Ag^0. The actual concentrations of AgNPs on the surface of NSP were determined by an atomic absorption spectrometer (iCE 3300; Thermo Scientific, Massachusett, USA). In addtion, physically produced AgNPs with ~5 nm nominal diameter (Global Nanotech Industries, Taiwan)[35] were used in this study for comparison. The sizes of AgNP/NSP were observed by a Hitachi H-7100 TEM (Tokyo, Japan) operated at 100 kV. Size distribution of AgNPs on the surface of NSP was computed by software based on the image. X-ray photoelectron spectroscopy (XPS, VG Scientific ESCALAB 250, U.K.) of Si 2p electron was used to obtain the information of Ag−Si interaction. The surface charge and hydrodynamic diameter were determined by a zeta potential and particle size analyzer (Delsa Nano S; Beckman Coulter, Osaka, Japan). The suspension of AgNP/NSP hybrids was first centrifuged at 16000× g for 30 min and the supernatant was collected. The supernatant was either directly measured (for Ag^+) or measured after dilution by 0.5 M HNO_3 solution (for both Ag^+ and AgNPs).[36] The concentration of release Ag^+ or free AgNPs in solution was determined by an atomic absorption spectrometer (iCE 3300; Thermo Scientific, Massachusett, USA).

2.2. Synthesis of Waterborne Poly(ether)urethane (PEU) and Preparation of PEU-AgNP/NSP Nanocomposites. Bis-(hydroxymethyl) propionic acid (DMPA) and the macrodiol poly-(tetramethylene oxide) (PTMO) were mixed at 50 °C in methyl ethyl ketone (MEK). After complete dispersion, dicyclohexylmethane diisocyanate (H_{12}MDI) and 4,4-diphenylmethane diisocyanate (MDI) were added to react at 75 °C. Triethylamine (TEA) was then added after the previous reaction was finished. Distilled water was introduced and isophorone diamine (IPDA) was finally added to complete the synthesis of PEU emulsion. Thick films for tests were made by pouring PEU emulsion and that containing AgNP/NSP 8/92, AgNP/NSP 1/99, or AgNPs into a Teflon mold. The content of Ag in all nanocomposites was 10 or 20 ppm. Each PEU-Ag nanocomposite was abbreviated as PEU-AgNP/NSP 8/92, PEU-AgNP/NSP 1/99, and PEU-AgNPs). The cast samples were dried in the vacuum at room temperature to remove any residual water in samples.

The surface morphology of PEU-Ag nanocomposites was examined by an atomic force microscope (AFM) (CP-II, Veeco, USA). The phase images were obtained in the tapping mode in air with a triangular cantilever (force constant of 20−80 N/m) supporting an integrated pyramidal tip of phosphorus-doped silicon (RTESPA-CP, Veeco, USA).

2.3. Cytotoxicity and Cell Attachment Tests. All cells used in this study were purchased from the Bioresource Collection and Research Center (Taiwan, ROC). Mouse skin fibroblast cells (L929), human hepatoma cells (HepG2) and murine macrophages (J774A1) were cultured in low-glucose Dulbecco's modified Eagles medium (DMEM) (Gibco, USA), high-glucose DMEM (Gibco, USA), and Minimum essential medium (MEM) (Gibco, USA), respectively. All media contained 10% fetal bovine serum (FBS) (SAFC Biosciences, USA), 1% Antibiotic-Antimycotic solution (Caisson, USA), and 1.5 g/L sodium bicarbonate (Sigma, USA). Cells were incubated at 37 °C under 5% CO_2. For cytotoxicity analysis, cells in a density of 5 × 10^4 per well were cultured in 24-well tissue culture plates. After 24 h, the medium was replaced by fresh medium containing AgNP/NSP, NSP or AgNPs at different concentrations (total weight). The culture medium was used as the negative control, whereas that containing 10% dimethyl sulfoxide (DMSO) (Sigma, USA) was used as the positive control. After 6, 12, or 24 h of treatment, cell viability was measured by the 3-(4,5-dimethylthiazol- 2-yl)-2,5- diphenyltetrazolium bromide (MTT) assay (Sigma, USA), which can be converted into formazan by mitochondrial enzymes in living cells. DMSO was then added to dissolve the purple formazan and the absorbance was measured at 550 nm by the UV−vis spectroscopy from a microplate reader (SpectraMax M5, Molecular Devices, USA). The median lethal concentration (LD_{50}) of each nanomaterials was obtained by multinomial regression models. The average size of J774A1 macrophages treated with AgNP/NSP, NSP, and AgNPs were measured by a particle counter (Multisizer3 Coulter Counter, Beckman Coulter, USA).

To evaluate the cytocompatibility of PEU-AgNP/NSP nanocomposites, the films (pure PEU, PEU-AgNP/NSP 8/92, PEU-AgNP/NSP 1/99, and PEU-AgNPs) were placed in 24-well tissue culture plates, where L929 fibroblasts were seeded in a density of 1 × 10^4 cells per well. The content of Ag in all nanocomposites was 20 ppm. After incubation for 24 or 72 h, the membranes were washed with PBS and the adherent cells were trypsinized for counting. For each group, four parallel samples were used in the cell attachment study.

2.4. Inflammatory Gene Expression by Reverse Transcription-Polymerase Chain Reaction (RT-PCR). J774A1 macrophages were incubated with AgNP/NSP, NSP, and AgNPs for 6 or 12 h, and were collected for extraction of total RNA. Cells were first disrupted in 1 mL of Trizol reagent (Invitrogen, USA), followed by an addition of 200 μL of chloroform (Tedia, USA) for extracting RNA. After centrifugation at 14000 rpm at 4 °C for 10 min, the aqueous

phase was removed and mixed with 500 μL of isopropanol (J.T. Baker, USA). The RNA was collected by centrifuging, and the pellet was washed with 75% ethanol/diethyl pyrocarbonate (DEPC) solution. RNase-freeDEPC-treated water was used to dissolve RNA, and the concentration of RNA was assessed by the Quant-iT Ribogreen RNA assay kit (Invitrogen, USA) on a Qubit Fluorometer (Invitrogen, USA). cDNA was synthesized with RevertAid First Strand cDNA Synthesis Kit (Fermentas, Germany). In PCR reaction, the primer sequence used for interlukin-1 (IL-1) was 5′CCCAAGCAATACC-CAAAGAAGAAG3′ (forward) and 5′TGTCCTGACCAC-TGTTGTTTCC3′ (reverse); the primer sequence used for interlukin-6 (IL-6) was 5′TTCCATCCAGTTGCCTTCTTG3′ (forward) and 5′TCATT TCCACGATTTCC- CAGAG3′ (reverse); the primer sequence used for tumor necrosis factor (TNF-α) was 5′CGAGTGACAAGCCTGTAGCC3′ (forward) and 5′TTGAAGA-GAACCTG- GGAGTAGAC3′ (reverse); the primer sequence used for β-actin was 5′ TCCTGTGGCATCCACGAAACT3′ (forward) and 5′ GGAGCAATGATCCTGA- TCTTC3′ (reverse). The PCR amplification was performed by a Thermal Cycler (GeneAmp PCR System 2700, Applied Biosystems, USA), and the level of gene expression was determined by the capillary electrophoresis with a 12-capillary gel-cartridge DNA screening kit (QIAxcel, Qiagen, Germany).

2.5. Hemolysis Assay. Hemoglobin standards (rabbit, Sigma, USA) were reacted with the Drabkin's reagent (Sigma, USA) and used to construct a standard curve covering the range from 0.022 to 1.4 mg/mL by a microplate reader at 540 nm. The whole blood was then collected from rabbits and the total blood hemoglobin was determined by the standard curve. One ml diluted whole blood (whole blood was diluted to 10 mg/mL by normal saline) was added into a tube with 7 mL of distilled water (as the positive control), normal saline (as the negative control), or the test samples (different concentrations of AgNP/NSP, NSP, and AgNPs in normal saline). All samples were incubated in a water bath at 37 °C for 3 h and centrifuged at 2400 rpm for 15 min. The concentration of released hemoglobin in supernatants was quantified by addition of Drabkin's reagent and measured at 540 nm. The hemolytic ratio was obtained by dividing the difference of absorbance between samples and negative control with that between positive and negative controls.

2.6. Antibacterial Activity. The antibacterial activity of AgNP/NSP was performed according to the American Society for Testing and Materials Standard (ASTM) E2315−03. The bacterial strain used for the experiment was *Escherichia coli* (*E. coli*), which was purchased from the Bioresource Collection and Research Center (Taiwan, ROC). Bacteria were grown in nutrient broth which contained 3 g beef extract (Himedia, India), 10 g peptone (BD Bioscience, USA), and 5 g sodium chloride (Sigma, USA) in 1 L of water, and cultured in a logarithmic phase of the growth curve. After dilution, the bacterial suspension (1×10^6 CFU/mlL) was adjusted to contain 10 ppm (final concentration) for AgNP/NSP 8/92, 63 ppm for AgNP/NSP 1/99, 63 ppm for NSP, or 0.82 ppm for AgNPs. Deionized water was also added into bacterial solution to serve as controls. The bacterial suspensions were grown in a shaker incubator at 35 °C and 110 rpm for 0 (immediately), 3, 6, 12, and 24 h. At each time point, the solutions were cooled and diluted serially for colony counting. Aliquots of diluted solution (100 μL) were spread on each agar plate. After incubation at 37 °C for 24 h, the CFU on the agar can be counted.

The microbiostasis ratio of the polymer nanocomposites followed the Japanese Industrial Standard (JIS) Z 2801. The bacterial strain used for the experiment was *Escherichia coli* (*E. coli*). The polymer nanocomposites (pure PEU, PEU-AgNP/NSP 8/92, PEU-AgNP/NSP 1/99, and PEU-AgNPs) were cut to square (5 cm × 5 cm). The content of Ag in all nanocomposites was 10 ppm. Sample films were placed in Petri dishes and inoculated with 400 μL of bacterial cell suspension (2.5×10^5 to 1×10^6 CFU/mL) at a temperature of 35 °C and a relative humidity of 90%. After an immediate contact (control) or 24 h of contact time, the residual bacteria were washed out and diluted serially for colony counting. Aliquots of diluted solution (100 μL) were spread on agar plates. After incubation at 37 °C for 24 h, colonies on the agar were counted visually and as CFU per sample. The bacterial growth inhibition was calculated by the following equation: antibacterial efficiency = $(N_0 - N)/N_0$, where N_0 and N each represents the bacteria number of control and experimental group.

3. RESULTS

3.1. Preparation and Characterization of AgNPs/NSP. Spherical AgNPs were prepared by reduction of $AgNO_3$ on the surface of exfoliated NSP (Figure 1). The actual weight ratio for

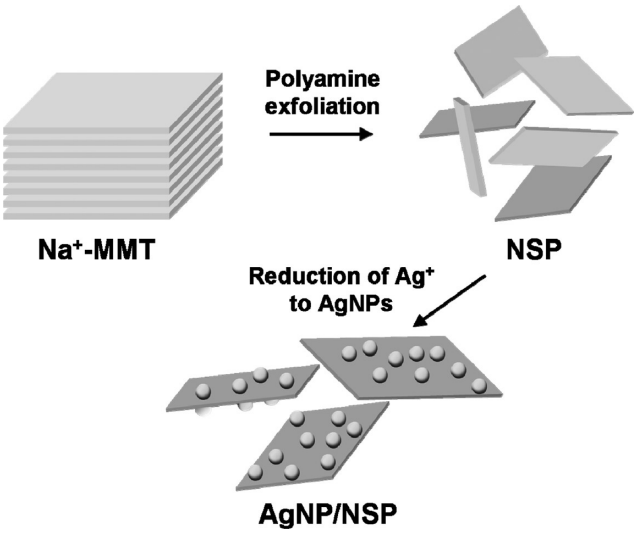

Figure 1. Preparation of AgNPs on NSP by chemical reduction.

AgNP/NSP 1/99 was 1.3/98.7, and that for AgNP/NSP 8/92 was 8.2/91.8. The AgNP/NSP hybrids had proper dispersion and particle size. The average diameter of AgNPs on the hybrid at 1/99 weight ratio was 4.60 ± 1.89 nm, whereas that at 8/92 weight ratio was 9.45 ± 2.67 nm, as visualized by TEM (Figure 2). According to Figure 2A, we clearly observed the coexistence of silica platelets and AgNPs in the field. Moreover, none of the free AgNPs was observed, indicating that only a limited amount of AgNPs were detached from the silicate platelets. XPS in Figure 2C provided information on Ag−Si interaction. High-resolution Si 2p spectra showed that there was interaction between Ag and Si in AgNP/NSP 8/92, causing a shift of binding energy from 105.6 eV (Si−O, NSP) to 105.1 eV. Further increase of the Ag content (Ag/NSP = 30/70) shifted this peak to 103 eV (data not shown). The hydrodynamic diameter measured by light scattering was 433.90 ± 60.80 nm for AgNP/NSP 1/99, 123.00 ± 28.90 nm for AgNP/NSP 8/92, 291.00 ± 92.40 nm for NSP, and 22.60 ± 7.80 nm for free AgNPs, respectively (Table 1). The surface charges of these nanomaterials were measured by zeta potential. AgNP/NSP and NSP were both negatively charged while AgNPs were positively charged. To avoid the cytotoxic effect caused by Ag^+, the weight ratio of nonreduced Ag^+ in the sample was measured by atomic absorption spectrometry. It was found that only a very limited amount (~170 ppb) of Ag^+ was present in the suspension of AgNP/NSP 8/92.

3.2. In vitro Cytotoxic Effect. The cytotoxic effect of AgNP/NSP based on the decrease of mitochondrial activities is shown in Figure 3. The cell viability upon exposure to the nanomaterials for 24 h was reduced in a dose-dependent manner. While the cytotoxicity of AgNP/NSP 1/99, AgNP/NSP 8/92, and NSP exhibited a similar trend, the dose-dependent cytotoxicity of AgNP/NSP 8/92 to L929 cells was

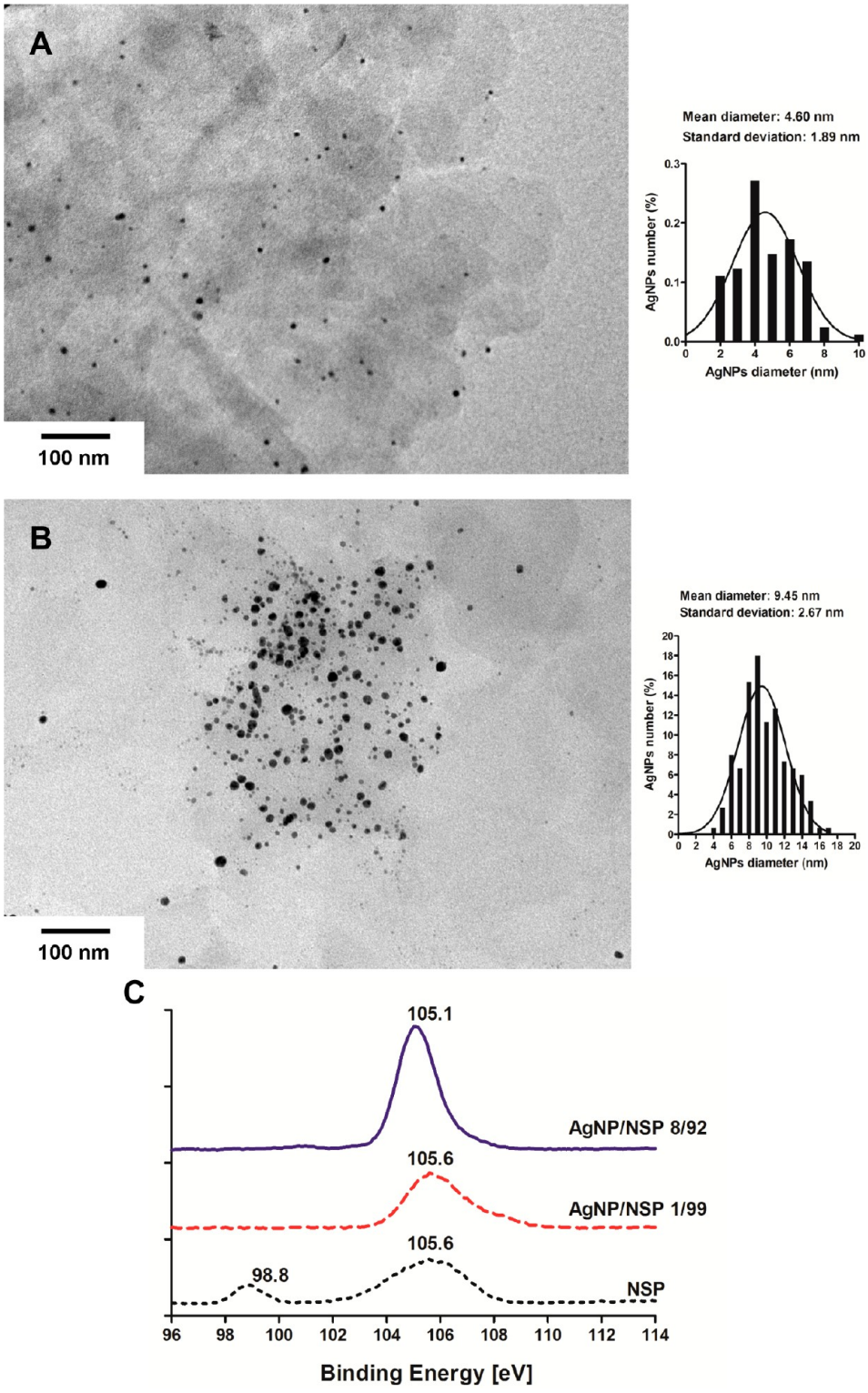

Figure 2. TEM images of (A) AgNP/NSP 1/99 and (B) AgNP/NSP 8/92. (C) XPS spectrum of AgNP/NSP 1/99, AgNP/NSP 8/92, and NSP.

the most obvious (Figure 3A). The LD_{50} of L929 cells obtained from the multinomial regression was 37.90 ppm for AgNP/NSP 1/99, 44.19 ppm for AgNP/NSP 8/92, 39.40 ppm for NSP, and 12.84 ppm for AgNPs. Compared to AgNP/NSP 8/92 and NSP, AgNP/NSP 1/99 presented similar cytotoxicity to L929 cells. Physically produced AgNPs decreased the mitochondrial activities of L929 slightly, and the cell viability was more than 75% in the concentration range from 0.13 to 8.2 ppm.

Figure 3B showed the cytotoxicity of nanomaterials to HepG2 cells after incubation for 24 h. AgNP/NSP 8/92 was significantly more toxic to HepG2 than NSP and AgNP/NSP 1/99. In the concentrations tested, NSP revealed a much lower cytotoxic effect to HepG2 cells vs L929 cells, and the HepG2 viability was over 90%. AgNP/NSP 1/99, moreover, demon-

dx.doi.org/10.1021/am302534k | ACS Appl. Mater. Interfaces 2013, 5, 433−443

Table 1. Zeta Potential and Particle Size of AgNP/NSP

specimens	size of silver nanoparticles (nm)	hydrodynamic diameter (nm)	zeta potential (mV)
AgNP/NSP 1/99	4.29 ± 1.16	433.90 ± 60.80	−41.51 ± 0.53
AgNP/NSP 8/92	9.45 ± 2.67	123.00 ± 28.90	−35.21 ± 1.12
NSP	n/a	291.00 ± 92.40	−59.88 ± 2.13
AgNPs	5.75 ± 1.12	22.60 ± 7.80	15.43 ± 2.72

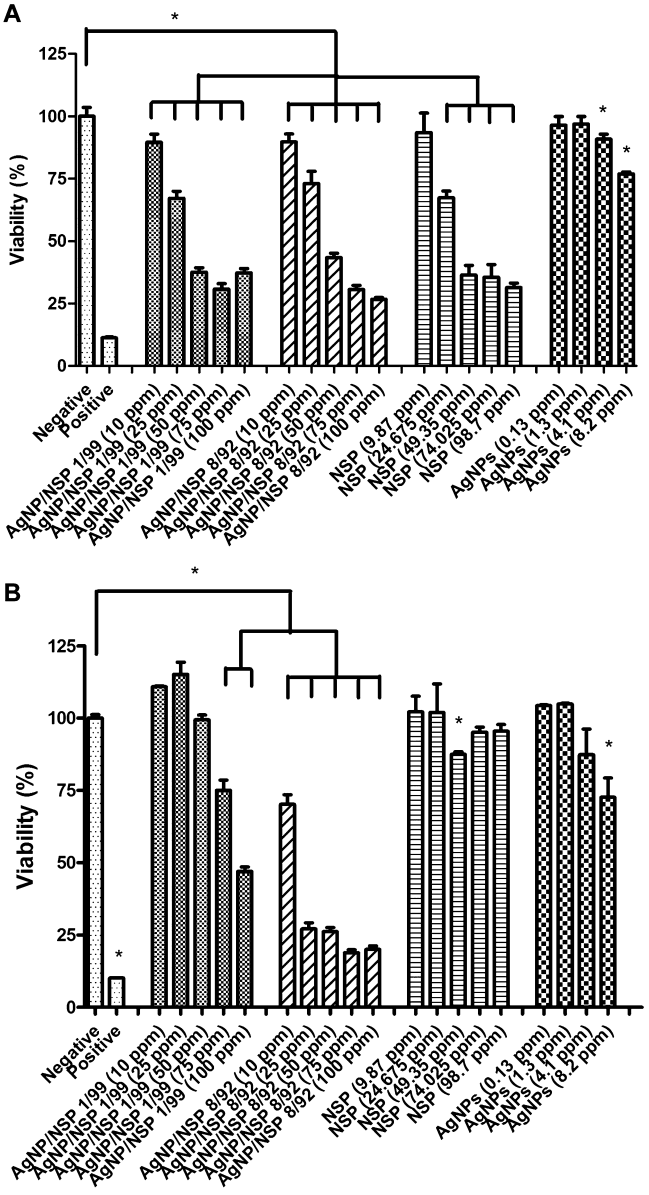

Figure 3. Cytotoxic effects of AgNP/NSP, NSP, and AgNPs on (A) L929 cells and (B) HepG2 cells. The concentration of NSP or AgNPs corresponded to the content of each component within the AgNP/NSP hybrid. The concentration was based on the total weight, e.g., AgNP/NSP 1/99 10 ppm contains 9.87 ppm NSP and 0.13 ppm AgNPs. * indicates a statistical difference from the control, $p < 0.05$.

strated higher viability of HepG2 vs L929 cells, which indicated that HepG2 cells possessed better tolerance to AgNP/NSP 1/99. The LD_{50} of HepG2 was 96.88 ppm for AgNP/NSP 1/99, 18.45 ppm for AgNP/NSP 8/92, and 14.13 ppm for AgNPs.

3.3. Immunological Response and Gene Expression of J774A1 Macrophages. Figure 4 shows the viability of J774A1 macrophages treated with AgNP/NSP, NSP, or AgNPs for 6 and 12 h. After 6 h of incubation, the number of macrophages in each group showed only slight difference from the negative control. Further exposure of 12 h induced more serious cell death in all of the treated groups, especially those treated with AgNP/NSP 1/99 and NSP (63 ppm). The average sizes of macrophages upon exposure to different nanomaterials are shown in Table 2. After 6 h, the size of macrophages in the group of AgNP/NSP 1/99 was about 0.52 μm larger than the control group, and that of NSP (63 ppm) was about 0.43 μm larger. After 12 h, the cell size was significantly larger in the groups of AgNP/NSP 1/99, AgNP/NSP 8/92, and NSP (63 ppm), and each was 0.5, 0.35, and 0.37 μm larger than negative control. The exposure of physically produced AgNPs (at the low concentration 0.82 ppm) did not increase the size of macrophages at both 6 and 12 h.

The proinflammatory gene expression of J774A1 macrophages treated with nanomaterials for 6 h is shown in Figure 5. The expression of tumor necrosis factor (TNF-α) gene in the control, NSP-treated, and AgNP/NSP-treated groups revealed no significant difference. In the same period, the expressions of interlukin-1 (IL-1) and interlukin-6 (IL-6) genes in AgNP/NSP- and AgNP-treated groups were only slightly higher than those of control.

3.4. Hemolysis Assay. The hemolytic ratios of RBCs upon exposure to AgNP/NSP, NSP, AgNPs, or Ag^+ for 3 h are listed in Table 3. At 10 ppm of AgNP/NSP or NSP, the hemolytic ratio was below 5%, which could be regarded as hemocompatible. As the concentration increased, AgNP/NSP 8/92 caused more significant RBC lysis compared to NSP and AgNP/NSP 1/99. AgNPs in the concentration range of 2−10 ppm also led to a dose-dependent hemolysis. Ag^+ at the concentration of 0.017 ppm (the estimated amount in AgNP/NSP suspension) did not induce any hemoglobin release.

3.5. Characterization of PEU−Ag Nanocomposites. SEM data showed that no AgNP/NSP nanohybrid was apparently observed on the surface of PEU (see Figure S1 in the Supporting Information), probably because of the small amount of the nanohybrid in the PEU matrix. On the other hand, AFM phase images provided better information regarding the surface change of PEU in the presence of the nanohybrid. Figure 7 shows AFM phase images for PEU as well as PEU-Ag nanocomposites. PEU, like most polyurethane, has a segmented structure, i.e. microphase separation. In AFM phase images, the hard segment-rich domain of PEU matrix was represented as the bright area, whereas the soft segment-rich domain presented as the dark area. AFM images showed that the soft and hard domains in the pristine PEU were regularly distributed. With the presence of AgNP/NSP 8/92 or AgNPs, the hard domains were significantly smaller and better-dispersed, indicating the microphase separation of PEU. When adding AgNP/NSP 1/99, the hard domains formed a delicate network, suggesting a more effective modulation of microphase separation by this AgNP/NSP hybrid.

3.6. Cell Attachment. The attachment and proliferation of L929 fibroblasts on PEU-Ag nanocomposites containing 20 ppm silver are shown in Figure 8. The attachment was evaluated at 24 h and proliferation was evaluated at 72 h. There was no significant difference in cell number among the groups at either 24 or 72 h. However, cells were obviously more after

dx.doi.org/10.1021/am302534k | ACS Appl. Mater. Interfaces 2013, 5, 433−443

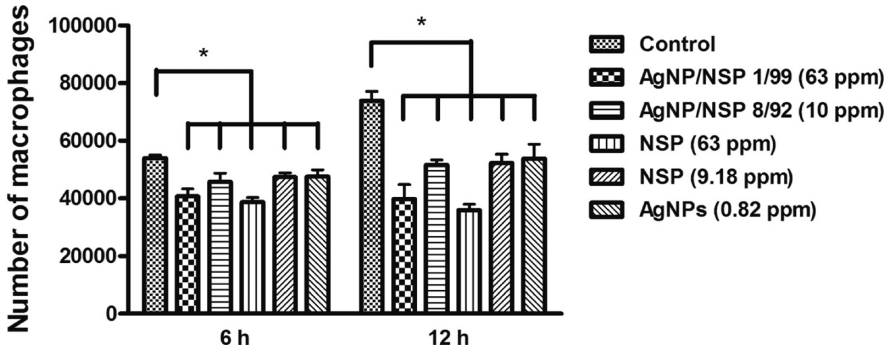

Figure 4. Cytotoxicity of AgNP/NSP, NSP, and AgNPs on J774 A1 macrophages. Cells were incubated with nanohybrids for 6 and 12 h. The concentration was based on the total weight. * indicates a statistical difference from the control, $p < 0.05$.

Table 2. Average Size of J774A1 Macrophages Treated with AgNP/NSP, NSP, and AgNPs

specimens	cell average size (μm)	
	6 h	12 h
control	14.33 ± 0.23	14.51 ± 0.15
AgNP/NSP 1/99 (63 ppm)	14.85 ± 0.26[a]	15.01 ± 0.63
AgNP/NSP 8/92 (10 ppm)	14.48 ± 0.25	14.86 ± 0.16[a]
NSP (63 ppm)	14.76 ± 0.17[a]	14.88 ± 0.36[a]
NSP (9.18 ppm)	14.45 ± 0.20[a]	14.64 ± 0.22
AgNPs (0.82 ppm)	14.36 ± 0.13	14.47 ± 0.34

[a]indicates a statistical difference from the control, $p < 0.05$.

72 h, indicating that cells kept growing on all materials during the period.

3.7. Antibacterial Activity. The antibacterial activities during the direct incubation of nanohybrids with *E. coli* are illustrated in Figure 6. The colony counts of *E. coli* in the NSP group showed only slight change during 24 h. However, the colony numbers in the groups of AgNP/NSP 1/99, AgNP/NSP 8/92, and AgNPs all decreased in a time-dependent manner. During the first 3 h, no significant difference was observed among each group. After 6 h, AgNP/NSP 1/99 showed 40% bacterial inhibition, whereas AgNPs displayed 12% bacterial inhibition. At 24 h, about 98.8% elimination of bacteria was observed in the group of AgNP/NSP 8/92. Complete inhibition of *E. coli* by 63 ppm of AgNP/NSP 1/99 was observed at 24 h. At each time point, AgNP/NSP in particular AgNP/NSP 1/99 showed a higher degree of bacterial inhibition, as compared with controls and physically produced AgNPs.

Figure 9 demonstrates the microbiostasis ratios of PEU-Ag nanocomposites containing either 20 ppm or 10 ppm silver against *E. coli*. In Figure 9A, the microbiostasis ratios of PEU and PEU-AgNPs (20 ppm silver) were both negative, indicating that the bacteria kept growing on the surface of the two materials during the period (24 h). On the other hand, the microbiostasis ratios of PEU-AgNP/NSP 1/99 and PEU-AgNP/NSP 8/92 both reached 99.9%. When the silver content was lowered to 10 ppm, the antibacterial activity showed a similar trend to that in Figure 9A, but the microbiostasis ratios of PEU-AgNP/NSP 1/99 and PEU-AgNP/NSP 8/92 were reduced to 96.0 and 97.0%, respectively. These results indicated that PEU-AgNP/NSP nanocomposites possessed much better microbiostatic ability than PEU-AgNP nanocomposites at equivalent silver concentrations.

4. DISCUSSION

Experimental evidence show that AgNPs, because of their ultrasmall size, can facilitate entry into tissues, cells, and biological molecules.[11,37,38] In particular, AgNPs with remarkable antimicrobial activities have increasing medical applications. Therefore, antimicrobial materials containing AgNPs are becoming increasingly important. In contrast, previous reports indicated that silver microparticles (AgMPs) are not able to get assess into cells.[38] The entry of silver particles is size-dependent. Furthermore, AgMPs with low reactive surface area possess significantly weaker inhibitory effect against bacteria, as compared with AgNPs.[39]

AgNPs with remarkable antimicrobial activities are the most potential nanomaterials in the biomedical field. Nevertheless, suspended AgNPs tend to aggregate together due to the ionic or van der Waals attraction among particles. This may affect their biological responses, including absorption, distribution, metabolism, excretion, as well as antibacterial properties.[5,9,40] Thus, a variety of chemicals such as surfactants, polymers, and ligands are extensively applied to prepare highly stable AgNP dispersions.[33,41,42] Previously we have synthesized a novel nanohybrid consisting of 10 or 20% AgNPs immobilized on NSP.[33] The AgNP/NSP hybrid dispersed well in solution and showed antibacterial potential. However, the proper parameters for preparing AgNP/NSP have not been fully investigated. AgNP/NSP hybrids with two different weight ratios (1/99 and 8/92) were prepared in this study. The cytotoxicity and antibacterial efficiency were further compared. It was in the hope that AgNP/NSP hybrids with the optimal dispersion and density would have lower cell toxicity while retain the antibacterial activities.

The single-layered NSPs are exfoliated from the MMT primary stacks and characterized as thin platelets with large surface area. With this property, the surface ionic charges of NSP can be fully exposed and interact with $AgNO_3$ initially and Ag^0 particles after the reduction of Ag^+.[43] Before the reduction, Ag^+ was exchanged with the counterions (Na^+) in the clay interlayer via ionic exchange mechanism, and then reduced to form AgNPs. To clarify whether the antibacterial activity and the cytotoxicity were predominately influenced by AgNP/NSP nanohybrids, the presence of released Ag^+ or free AgNPs was measured. It was found that only 170 ppb Ag^+ and 270 ppb free AgNPs presented in the suspension of AgNP/NSP 8/92. In our previous study, we also demonstrated that only 356 ppb Ag^+ and 39 ppb free AgNPs was presented in 1.0 wt % AgNP/NSP suspension.[33] Moreover, after 6 months of storage, the supernatant of AgNP/NSP hybrids showed no antibacterial

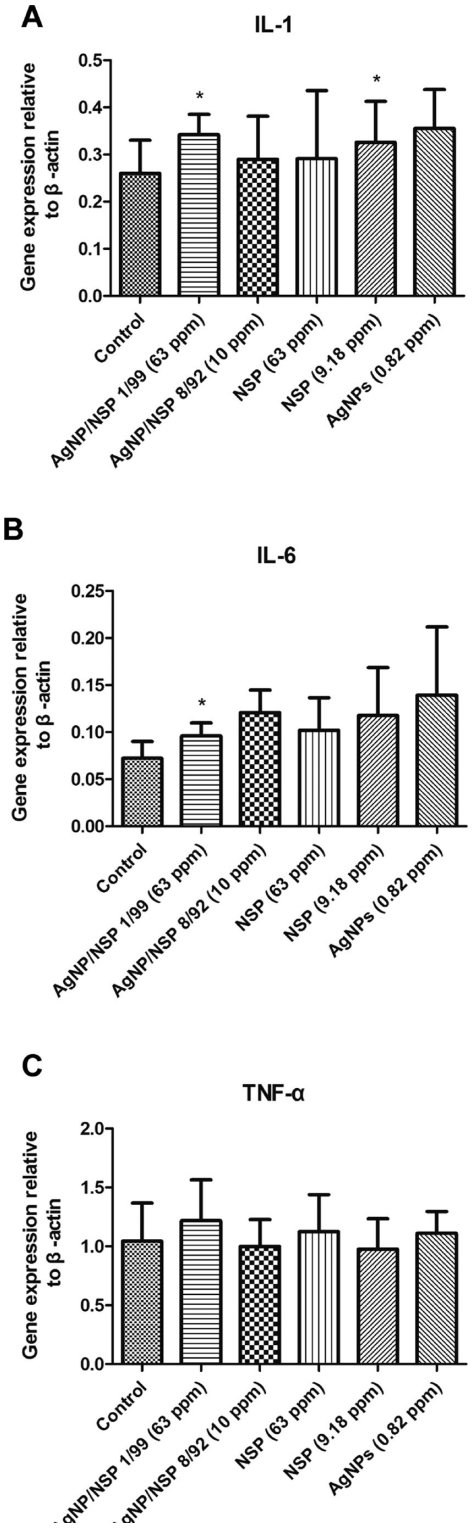

Figure 5. The gene expression of IL-1, IL-6, and TNF-α in J774A1 macrophages incubated with AgNP/NSP, NSP, and AgNPs for 6 h. The concentration was based on the total weight. * indicates a statistical difference from the control, $p < 0.05$.

activity. The results strongly suggested that the biocidal effect was mainly induced by the immobilized AgNPs on NSP.

The TEM images indicated that the diameter and dispersion of AgNPs depended on the ratio of $AgNO_3$ to NSP. A higher concentration of $AgNO_3$ led to AgNPs of larger size on the hybrid. According to literature, the antibacterial activity of AgNPs is size-dependent.[5,44] AgNPs in smaller size may provide more surface area for bacterial contact and induce more growth inhibition. Because of the self-assembly nature of NSP, the hydrodynamic diameters of NSP and AgNP/NSP hybrids were greater that those based on TEM. The zeta potential measurement confirmed the good stability of NSP and AgNP/NSP hybrids.

Cytotoxicity results revealed that the three cell lines (L929 fibroblasts, HepG2 cells, and J774A1 macrophages) used in this study exhibited different extents of tolerance to the nanomaterials. For L929 fibroblasts and J774A1 macrophages, their viability was predominately governed by the concentration of NSP. The decrease of HepG2 cell viability was strongly associated with the density of AgNPs. The difference may be attributed to the various natures of these cells. Compared with the other two, HepG2 cells tend to gather for growth, which present less cell-material contact. Many studies have demonstrated that AgNPs may induce significant cytotoxicity both in vitro and in vivo.[45−47] The AgNP-induced cytotoxicity has been attributed to the generation of ROS and oxidative stress.[11,12,48] Although a previous study suggested that NSP were biocompatible to human gingival fibroblasts and bovine endothelial cells at the concentration of 10 ppm,[49] the current results revealed that the toxicity of NSP may vary with different cell types. A recent study[32] has investigated the genotoxic effect of NSP by the Ames test, Comet assay, and micronucleus assay. It was reported that no gene mutations of bacteria was observed after incubation with 1000 μg NSP per plate, no DNA damage of CHO cells within 1000 ppm NSP, and no chromosomal damage in ICR mice at doses of 500 mg NSP/kg. Because of the geometric feature of NSP, immobilized AgNPs do not enter cells readily, which warrants the biosafety of AgNP/NSP hybrids for further clinical use. The result of negative mutagenicity from the Ames test of AgNP/NSP hybrids also suggests the lack of genotoxicity (see Table S1 in the Supporting Information).

The response of inflammatory cells to AgNP/NSP hybrids is another essential concern. Macrophages are one of the principal cells that can be activated during the inmmunological response of NPs.[35,50] As macrophages undergo morphological transition from nonactivated to activated form, they expand their size.[51,52] The inflammatory responses as well as proinflammatory gene expressions of macrophages upon exposure to NSP, AgNPs, or AgNP/NSP hybrids were thus investigated. Compared with the regular macrophages, AgNP/NSP 1/99, AgNP/NSP 8/92, or NSP-treated macrophages showed larger size after 12 h exposure. This observation suggested activation of inflammatory responses. Those treated with AgNPs, on the other hand, did not increase their size significantly in the exposure period. The exposure of NSP, AgNPs or AgNP/NSP hybrids for 12 h did not upregulate the proinflammatory IL-1, IL-6, and TNF-α genes of macrophages. Taken together, these results propose that the treatment of NSP and AgNP/NSP hybrids may merely elicit a mild immune reaction.

The blood compatibility of nanomaterials is especially important when the biomedical applications involved possible contact with blood. When RBCs are damaged, the hemoglobin would release and hemolysis can be observed. Therefore, the hemolysis ratio is a representative index associated with the biocompatibility of blood contacting biomaterials.[53−55] In our study, both NSP and AgNP/NSP hybrids did not cause severe hemolytic activity at the concentration of 10 ppm (hemolysis $\leq$5% was permissible for biomaterials).[56] When the concen-

Table 3. Hemolytic Ratio of RBCs Treated with AgNP/NSP, NSP, AgNPs, and Ag^+. Ag^+ was Present in Dissolved $AgNO_3$

	hemolytic ratio (%)				
overall concentration (ppm)	AgNP/NSP 8/92	AgNP/NSP 1/99	NSP	AgNPs	Ag^+
0.017	n/a	n/a	n/a	n/a	0.00 ± 0.42
2	n/a	n/a	n/a	0.00 ± 0.00	n/a
5	n/a	n/a	n/a	23.54 ± 0.22	n/a
10	2.69 ± 0.45	2.35 ± 0.11	2.24 ± 0.00	85.03 ± 0.24	n/a
25	73.54 ± 2.69	29.28 ± 2.61	16.14 ± 0.45	n/a	n/a
50	88.79 ± 1.35	59.40 ± 1.45	57.85 ± 0.90	n/a	n/a
100	97.31 ± 0.00	87.68 ± 3.33	82.96 ± 0.45	n/a	n/a

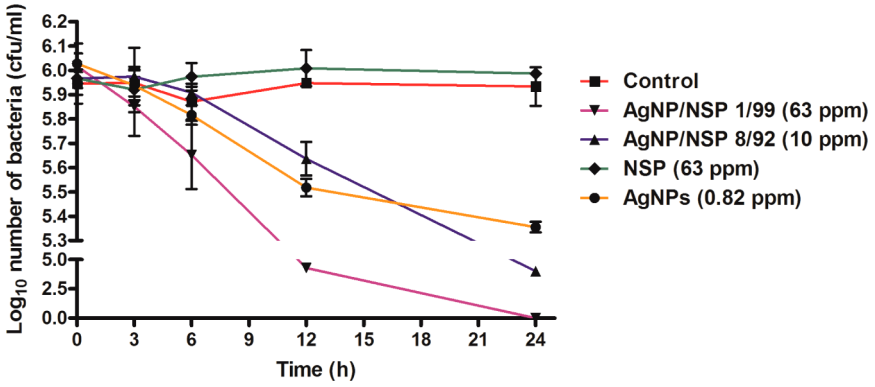

Figure 6. Antibacterial activities of NSP, AgNPs, and AgNP/NSP at 1/99 and 8/92 weight ratio against *E. coli* after different time of exposure. The concentration was based on the total weight. The antibacterial efficiency was 99.9% for AgNP/NSP 1/99, 98.8% for AgNP/NSP 8/92, and 73.6% for physically produced AgNPs after 24 h of incubation.

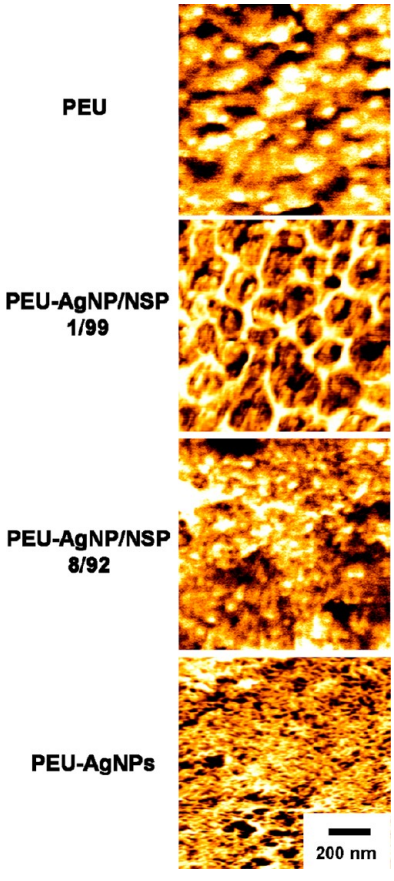

Figure 7. AFM phase images for PEU-Ag nanocomposites. The concentration of Ag was 20 ppm in PEU-AgNP/NSP 1/99 and PEU-AgNP/NSP 8/92, and 15 ppm in PEU-AgNPs [the latter from ref 44].

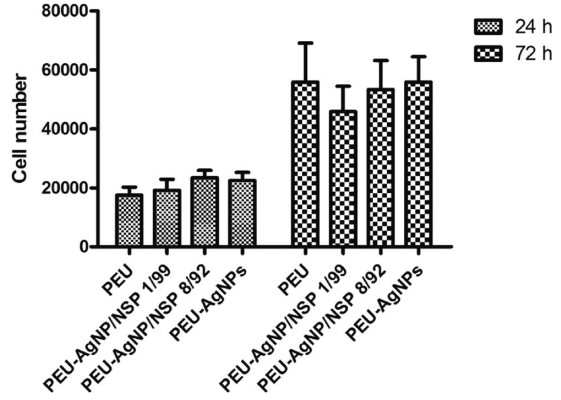

Figure 8. The growth of L929 fibroblasts on PEU and three different PEU-Ag nanocomposites (PEU-AgNP/NSP 1/99, PEU-AgNP/NSP 8/92, and PEU-AgNPs) at 24 h (attachment) and 72 h (proliferation). The concentration of Ag in all nanocomposites was 20 ppm.

tration was raised to 25 ppm, the membrane-damaging extent of NSP and AgNP/NSP hybrids significantly increased, especially for AgNP/NSP 8/92. This suggested that the AgNPs (silver content 2 ppm) on AgNP/NSP 8/92 may be responsible for the observed hemolysis. The impact of AgNPs on hemolysis has been widely investigated. Asharani et al. reported that the AgNPs generated ROS may induce severe lipid peroxidation, and further led to hemolysis and hemagglutination.[55] The hemolysis ratios of NSP, AgNPs, or AgNP/NSP hybrids all increased in a dose-dependent manner. As to NSP, various explanations for the hemolytic properties of silica materials have been mentioned, including the ROS production,[57] the protein denaturation induced by the affinity with silicat,[58] and the strong electrostatic interactions between surface silanols and the membrane trimethyl-ammonium head

dx.doi.org/10.1021/am302534k | ACS Appl. Mater. Interfaces 2013, 5, 433−443

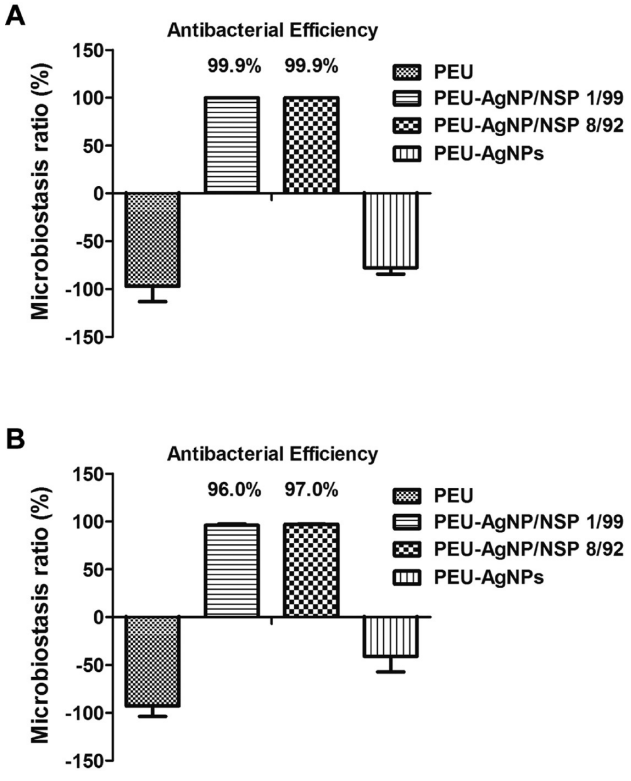

Figure 9. Microbiostasis ratios of PEU and three different PEU-Ag nanocomposites (i.e., PEU-AgNP/NSP 1/99, PEU-AgNP/NSP 8/92, and PEU-AgNPs) against *E. coli*. The concentration of Ag in all nanocomposites was (a) 20 ppm and (b) 10 ppm.

groups.[53] Although the mechanism of silicate-induced hemolysis is not completely understood, many recent reports have shown that the hemolytic effect of silica is strongly related to the density of surface silanol groups.[53,59,60]

The AgNP/NSP hybrids were examined for their antibacterial effect in aqueous suspension at 0.82 ppm silver content by direct incubation with *E. coli*. The antibacterial activity of the nanomaterials ranked as: AgNP/NSP 1/99 > AgNP/NSP 8/92 > AgNPs > NSP. It was noted that NSP alone did not significantly inhibit the growth of *E. coli* in the aqueous state. According to a previous study, the minimum bactericidal concentration of NSP was 3.0 wt % (equivalent to 30 000 ppm) in LB medium,[61] which is much higher than the amount of NSP (i.e., 63 ppm) tested in this study. Therefore, NSP did not seem to account for the antibacterial activity of AgNP/NSP hybrids. The extremely low amount of silver ions leached from the AgNP/NSP hybrids was not responsible for the antibacterial effect either. The bacterial growth reduction observed in this study was mainly brought about by the AgNPs. The mechanism of the antibacterial activity of AgNP/NSP hybrids may involve NSP physical-trapping effect due to their intensive ionic charges and the extensive interaction between AgNPs and bacteria.[19,33,61] The immobilized AgNPs do not penetrate into bacteria but are adsorbed only on the bacterial surface, gradually destroying the metabolic responses of cells.[10,62] Especially, the AgNP-induced ROS production is widely recognized as a major reason for cell death.[11,12] AgNP/NSP, in particular AgNP/NSP 1/99, showed better antibacterial efficiency, as compared with the free AgNPs. We assumed that NSP-stabilized AgNPs may offer higher surface density to contact with bacteria more efficiently. Therefore, AgNP/NSP hybrids with lower silver content are sufficient enough to trigger bacterial elimination. In AgNP/NSP 1/99 and AgNP/NSP 8/92, the distinctive tolerance levels of *E. coli* on AgNPs were ascribed to the different particle size.[44]

AgNP/NSP hybrids are strong bactericidal agents but they also show obvious cytotoxic effect, based on our results. Embedding these hybrids in a polymer matrix may largely increase their biosafety. Therefore, we blended AgNP/NSP 1/99, AgNP/NSP 8/92, or free AgNPs into waterborne PEU, and examined their cytotoxicity and antibacterial activity. PEU has been widely used as biomedical materials because of its good biocompatibility and mechanical properties,[63] yet with the concern of biostability raised for many years.[64] Previous studies showed that incorporating AgNPs to waterborne PEU may enhance the biostability as well as antimicrobial activity.[34,65] For the nanocomposites, our earlier report has investigated the amount of leaching silver in PU-AgNPs nanocomposites.[34] Extraction study of PU-Ag nanocomposites by nutrient media showed only 0.08−0.39 ppb Ag^+ and 0.07−0.18 ppb free AgNPs were extracted from PU-AgNPs, which caused no bacterial inhibition.

With regard to the variation of surface microstructure, our previous study showed that the addition of AgNPs in different sizes and concentrations may affect the distribution of hard and soft segment domains (i.e., microphase separation) of PEU matrix.[44] AgNPs in smaller size induced the surface morphological change of PEU more efficiently than those in larger size. However, this effect diminished when AgNPs were overloaded and aggregated. We have concluded that the dispersion of nanomaterials and the extra charges on the PEU ionomer critically determine the microphase separation. It was also revealed that the extent of surface microphase separation was correlated with biocompatibility. In another study, we investigated the distribution of AgNPs in polyurethane by TEM.[34] Most AgNPs were distributed near the interface between hard and soft domains. Thus, the changes of surface microstructure may be ascribed to the ability of AgNPs to modify the interfacial energy between hard and soft segments of polyurethane. Therefore, AgNPs in aggregation state failed to govern the surface microphase separation. In this study, the AFM phase images of PEU-Ag nanocomposites were very distinct from that of PEU. More delicate structures were observed in all nanocomposites, especially in PEU-AgNP/NSP 1/99. The more obvious change in the surface morphology of PEU-AgNP/NSP 1/99 was probably attributed to the non-aggregated and smaller AgNPs on NSP. In addition, the well-dispersed AgNPs with smaller size also demonstrated a greater antibacterial activity based on literature.

In this study, L929 fibroblasts kept proliferating on all PEU nanocomposites for 72 h, suggesting noncytotoxicity and good biocompatibility of the nanocomposites. At a low silver level (20 ppm), both PEU-AgNP/NSP 1/99 and PEU-AgNP/NSP 8/92 exhibited nearly complete bacterial growth reduction (99.9%). PEU-AgNPs, on the other hand, did not display such an effect at such a low silver level. The antibacterial activity may be limited by the dispersion and density of AgNPs in PEU matrix. Further decreasing silver to 10 ppm in nanocomposites still could not tell which hybrid (1/99 or 8/92) was more effective in eliminating bacteria. We hypothesized that embedding AgNP/NSP hybrids in PEU may diminish their difference in antibacterial effects.

5. CONCLUSION

In conclusion, two different weight ratios of AgNP/NSP hybrids with mild inflammatory response and outstanding antibacterial activity were developed. The AgNP/NSP hybrids were further embedded in polyurethane to reduce their cytotoxicity. In our study, the polyurethane-AgNP/NSP nanocomposites were biocompatible to mammalian cells but simultaneously retain the antibacterial effect. Our results warrant the biosafety of the nanocomposites for further clinical use. We expected that this surface modification approach would be served as a coating material for medical devices, such as catheters and vascular stents in the future.

■ ASSOCIATED CONTENT

Ⓢ Supporting Information

Genotoxicity test of AgNP/NSP on *Salmonella typhimurium* (Table S1) and SEM images (Figure S1). This material is available free of charge via the Internet at http://pubs.acs.org/.

■ AUTHOR INFORMATION

Corresponding Author

*Tel: 886-2-33665313. Fax: 886-2-33665237. E-mail: shhsu@ntu.edu.tw.

Notes

The authors declare no competing financial interest.

■ ACKNOWLEDGMENTS

This research was supported by the National Research Program for Nanoscience and Technology sponsored by the National Science Council (100-2120-M-002-006).

■ REFERENCES

(1) Chaloupka, K.; Malam, Y.; Seifalian, A. M. *Trends Biotechnol.* **2010**, *28*, 580−588.
(2) Payne, J. L.; Ambrosio, A. M. *J. Biomed. Mater. Res., Part B* **2009**, *89*, 217−222.
(3) Alt, V.; Bechert, T.; Steinrücke, P.; Wagener, M.; Seidel, P.; Dingeldein, E.; Domann, E.; Schnettler, R. *Biomaterials* **2004**, *25*, 4383−4391.
(4) Morones, J. R.; Elechiguerra, J. L.; Camacho, A.; Holt, K.; Kouri, J. B.; Ramírez, J. T.; Yacaman, M. J. *Nanotechnology* **2005**, *16*, 2346−2353.
(5) Lok, C. N.; Ho, C. M.; Chen, R.; He, Q. Y.; Yu, W. Y.; Sun, H.; Tam, P. K.; Chiu, J. F.; Che, C. M. *JBIC, J. Biol. Inorg. Chem.* **2007**, *12*, 527−534.
(6) Shrivastava, S.; Bera, T.; Roy, A.; Singh, G.; Ramachandrarao, P.; Dash, D. *Nanotechnology* **2007**, *18*, 225103−225111.
(7) Teow, Y.; Asharani, P. V.; Hande, M. P.; Valiyaveettil, S. *Chem. Commun. (Cambridge, U. K.)* **2011**, *47*, 7025−7038.
(8) Feng, Q. L.; Wu, J.; Chen, G. Q.; Cui, F. Z.; Kim, T. N.; Kim, J. O. *J. Biomed. Mater. Res.* **2000**, *52*, 662−668.
(9) Sondi, I.; Salopek-Sondi, B. *J. Colloid Interface Sci.* **2004**, *275*, 177−182.
(10) Kim, J. S.; Kuk, E.; Yu, K. N.; Kim, J. H.; Park, S. J.; Lee, H. J.; Kim, S. H.; Park, Y. K.; Park, Y. H.; Hwang, C. Y.; Kim, Y. K.; Lee, Y. S.; Jeong, D. H.; Cho, M. H. *Nanomedicine* **2007**, *3*, 95−101.
(11) Carlson, C.; Hussain, S. M.; Schrand, A. M.; Braydich-Stolle, L. K.; Hess, K. L.; Jones, R. L.; Schlager, J. J. *J. Phys. Chem. B* **2008**, *112*, 13608−13619.
(12) AshaRani, P. V.; Low, Kah.; Mun, G.; Hande, M. P.; Valiyaveettil, S. *ACS Nano* **2009**, *3*, 279−290.
(13) Martínez-Gutierrez, F.; Thi, E. P.; Silverman, J. M.; de Oliveira, C. C.; Svensson, S. L.; Vanden Hoek, A.; Sánchez, E. M.; Reiner, N. E.; Gaynor, E. C.; Pryzdial, E. L.; Conway, E. M.; Orrantia, E.; Ruiz, F.; Av-Gay, Y.; Bach, H. *Nanomedicine* **2012**, *8*, 328−336.
(14) Debnath, D.; Kim, C.; Kim, S. H.; Geckeler, K. E. *Macromol. Rapid Commun.* **2010**, *31*, 549−553.
(15) Ananth, A. N.; Daniel, S. C.; Sironmani, T. A.; Umapathi, S. *Colloids Surf., B* **2011**, *85*, 138−144.
(16) Radziuk, D.; Skirtach, A.; Sukhorukov, G.; Shchukin, D.; Möhwald, H. *Macromol. Rapid Commun.* **2007**, *28*, 848−855.
(17) Darroudi, M.; Ahmad, M. B.; Zamiri, R.; Zak, A. K.; Abdullah, A. H.; Ibrahim, N. A. *Int. J. Nanomedicine* **2011**, *6*, 677−681.
(18) Raveendran, P.; Fu, J.; Wallen, S. L. *J. Am. Chem. Soc.* **2003**, *125*, 13940−13941.
(19) Su, H. L.; Chou, C. C.; Hung, D. J.; Lin, S. H.; Pao, I. C.; Lin, J. H.; Huang, F. L.; Dong, R. X.; Lin, J. J. *Biomaterials* **2009**, *30*, 5979−5987.
(20) Foldbjerg, R.; Dang, D. A.; Autrup, H. *Arch. Toxicol.* **2011**, *85*, 743−750.
(21) Ariga, K.; Vinu, A.; Yamauchi, Y.; Ji, Q.; Hill, J. P. *Bull. Chem. Soc. Jpn.* **2012**, *85*, 1−32.
(22) Tang, F.; Li, L.; Chen, D. *Adv. Mater.* **2012**, *24*, 1504−1534.
(23) Li, Z.; Barnes, J. C.; Bosoy, A.; Stoddart, J. F.; Zink, J. I. *Chem. Soc. Rev.* **2012**, *41*, 2590−2605.
(24) Gai, F.; Zhou, T.; Zhang, L.; Li, X.; Hou, W.; Yang, X.; Li, Y.; Zhao, X.; Xu, D.; Liu, Y.; Huo, Q. *Nanoscale* **2012**, *4*, 6041−6049.
(25) Tsai, C. P.; Hung, Y.; Chou, Y. H.; Huang, D. M.; Hsiao, J. K.; Chang, C.; Chen, Y. C.; Mou, C. Y. *Small* **2008**, *4*, 186−191.
(26) Yang, P.; Gai, S.; Lin, J. *Chem. Soc. Rev.* **2012**, *41*, 3679−3698.
(27) Lin, F. H.; Lee, Y. H.; Jian, C. H.; Wong, J. M.; Shieh, M. J.; Wang, C. Y. *Biomaterials* **2002**, *23*, 1981−1987.
(28) Katti, D. R.; Ghosh, P.; Schmidt, S.; Katti, K. S. *Biomacromolecules* **2005**, *6*, 3276−3282.
(29) Lin, F. H.; Chen, C. H.; Cheng, W. T.; Kuo, T. F. *Biomaterials* **2006**, *27*, 3333−3338.
(30) Chu, C. C.; Chiang, M. L.; Tsai, C. M.; Lin, J. J. *Macromolecules* **2005**, *38*, 6240−6243.
(31) Lin, J. J.; Chu, C. C.; Chiang, M. L.; Tsai, W. C. *J. Phys. Chem. B* **2006**, *110*, 18115−18120.
(32) Li, P. R.; Wei, J. C.; Chiu, Y. F.; Su, H. L.; Peng, F. C.; Lin, J. J. *ACS Appl. Mater. Interfaces* **2010**, *2*, 1608−1613.
(33) Su, H. L.; Lin, S. H.; Wei, J. C.; Pao, I. C.; Chiao, S. H.; Huang, C. C.; Lin, S. Z.; Lin, J. J. *PLoS One* **2011**, *6*, e21125.
(34) Hsu, S. H.; Tseng, H. J.; Lin, Y. C. *Biomaterials* **2010**, *31*, 6796−6808.
(35) Yen, H. J.; Hsu, S. H.; Tsai, C. L. *Small* **2009**, *5*, 1553−1561.
(36) Ndung'u, K.; Ranville, M. A.; Franks, R. P.; Flegal, A. R. *Mar. Chem.* **2006**, *98*, 109−20.
(37) AshaRani, P. V.; Hande, M. P.; Valiyaveettil, S. *BMC Cell Biol.* **2009**, *10*, 65.
(38) Wei, L. N.; Tang, J. L.; Zhang, Z. X.; Chen, Y. M.; Zhou, G.; Xi, T. F. *Biomed. Mater.* **2010**, *5*, 044103.
(39) Sivolella, S.; Stellini, E.; Brunello, G.; Gardin, C.; Ferroni, L.; Bressan, E.; Zavan, B. *J. Nanomater.* **2012**, *2012*, 975842.
(40) Martinez-Gutierrez, F.; Olive, P. L.; Banuelos, A.; Orrantia, E.; Nino, N.; Sanchez, E. M.; Ruiz, F.; Bach, H.; Av-Gay, Y. *Nanomedicine* **2010**, *6*, 681−688.
(41) Lin, J. J.; Lin, W. C.; Dong, R. X.; Hsu, S. H. *Nanotechnology* **2012**, *23*, 065102.
(42) Bae, E.; Park, H. J.; Park, J.; Yoon, J.; Kim, Y.; Choi, K.; Yi, J. *Bull. Korean Chem. Soc.* **2011**, *32*, 613−619.
(43) Dong, R. X.; Chou, C. C.; Lin, J. J. *J. Mater. Chem.* **2009**, *19*, 2184−2188.
(44) Liu, H. L.; Dai, S. A.; Fu, K. Y.; Hsu, S. H. *Int. J. Nanomedicine* **2010**, *5*, 1017−1028.
(45) Greulich, C.; Diendorf, J.; Gessmann, J.; Simon, T.; Habijan, T.; Eggeler, G.; Schildhauer, T. A.; Epple, M.; Köller, M. *Acta Biomater.* **2011**, *7*, 3505−3514.
(46) Hackenberg, S.; Scherzed, A.; Kessler, M.; Hummel, S.; Technau, A.; Froelich, K.; Ginzkey, C.; Koehler, C.; Hagen, R.; Kleinsasser, N. *Toxicol. Lett.* **2011**, *201*, 27−33.

(47) Lankveld, D. P.; Oomen, A. G.; Krystek, P.; Neigh, A.; Troost-de, Jong. A.; Noorlander, C. W.; Van Eijkeren, J. C.; Geertsma, R. E.; De Jong, W. H. *Biomaterials* **2010**, *31*, 8350−8361.
(48) Park, E. J.; Yi, J.; Kim, Y.; Choi, K.; Park, K. *Toxicol. In Vitro* **2010**, *24*, 872−878.
(49) Hsu, S. H.; Tseng, H. J.; Hung, H. S.; Wang, M. C.; Hung, C. H.; Li, P. R.; Lin, J. J. *ACS Appl. Mater. Interfaces* **2009**, *1*, 2556−2564.
(50) Lucarelli, M.; Gatti, A. M.; Savarino, G.; Quattroni, P.; Martinelli, L.; Monari, E.; Boraschi, D. *Eur. Cytokine Network* **2004**, *15*, 339−346.
(51) Gordon, S.; Taylor, P. R. *Nat. Rev. Immunol.* **2005**, *5*, 953−964.
(52) Hsu, S. H.; Tang, C. M.; Tseng, H. J. *Acta Biomater.* **2008**, *4*, 1797−1808.
(53) Slowing, I. I.; Wu, C. W.; Vivero-Escoto, J. L.; Lin, V. S. *Small* **2009**, *5*, 57−62.
(54) Díaz, B.; Sánchez-Espinel, C.; Arruebo, M.; Faro, J.; de Miguel, E.; Magadán, S.; Yagüe, C.; Fernández-Pacheco, R.; Ibarra, M. R.; Santamaría, J.; González- Fernández, A. *Small* **2008**, *4*, 2025−2034.
(55) Asharani, P. V.; Sethu, S.; Vadukumpully, S.; Zhong, S. P.; Lim, C. T.; Hande, M. P.; Valiyaveettil, S. *Adv. Funct. Mater.* **2010**, *20*, 1233−1242.
(56) Autian, J. In *Polymers in Medicine and Surgery*; Kronenthal, R. L., Oser, Z., Martin, E., Eds.; Plenum Press: New York, 1975; Vol. *8*, pp 181−203.
(57) Nash, T.; Allison, A. C.; Harington, J. S. *Nature* **1966**, *210*, 259−261.
(58) Diociaiuti, M.; Bordi, F.; Gataleta, L.; Baldo, G.; Crateri, P.; Paoletti, L. *Environ. Res.* **1999**, *80*, 197−207.
(59) Gerashchenko, B. I.; Gun'ko, V. M.; Gerashchenko, I. I.; Mironyuk, I. F.; Leboda, R.; Hosoya, H. *Cytometry* **2002**, *49*, 56−61.
(60) Murashov, V.; Harper, M.; Demchuk, E. *J. Occup. Environ. Hyg.* **2006**, *3*, 718−723.
(61) Wei, J. C.; Yen, Y. T.; Su, H. L.; Lin, J. J. *J. Phys. Chem. C* **2011**, *115*, 18770−18775.
(62) Cho, K. H.; Park, J. E.; Osaka, T.; Park, S. G. *Electrochim. Acta* **2005**, *51*, 956−960.
(63) Briganti, E.; Losi, P.; Raffi, A.; Scoccianti, M.; Munao, A.; Soldani, G. *J. Mater. Sci.: Mater. Med.* **2006**, *17*, 259−266.
(64) Ward, B.; Anderson, J.; McVenes, R.; Stokes, K. *J. Biomed. Mater. Res.* **2006**, *79*, 827−835.
(65) Chou, C.; Hsu, S.; Chang, H.; Tseng, S.; Lin, H. *Polym. Degrad. Stab.* **2006**, *91*, 1017−1024.